BIOCHEMISTRY
including biophysical chemistry & molecular biology

Article

pubs.acs.org/biochemistry

Structural Organization of FtsB, a Transmembrane Protein of the Bacterial Divisome

Loren M. LaPointe, Keenan C. Taylor, Sabareesh Subramaniam, Ambalika Khadria, Ivan Rayment, and Alessandro Senes*

Department of Biochemistry, University of Wisconsin-Madison, 433 Babcock Drive, Madison Wisconsin, 53706, United States

Supporting Information

ABSTRACT: We report the first structural analysis of an integral membrane protein of the bacterial divisome. FtsB is a single-pass membrane protein with a periplasmic coiled coil. Its heterologous association with its partner FtsL represents an essential event for the recruitment of the late components to the division site. Using a combination of mutagenesis, computational modeling, and X-ray crystallography, we determined that FtsB self-associates, and we investigated its structural organization. We found that the transmembrane domain of FtsB homo-oligomerizes through an evolutionarily conserved interaction interface where a polar residue (Gln 16) plays a critical role through the formation of an interhelical hydrogen bond. The crystal structure of the periplasmic domain, solved as a fusion with Gp7, shows that 30 juxta-membrane amino acids of FtsB form a canonical coiled coil. The presence of conserved Gly residue in the linker region suggests that flexibility between the transmembrane and coiled coil domains is functionally important. We hypothesize that the transmembrane helices of FtsB form a stable dimeric core for its association with FtsL into a higher-order oligomer and that FtsL is required to stabilize the periplasmic domain of FtsB, leading to the formation of a complex that is competent for binding to FtsQ, and to their consequent recruitment to the divisome. The study provides an experimentally validated structural model and identifies point mutations that disrupt association, thereby establishing important groundwork for the functional characterization of FtsB *in vivo*.

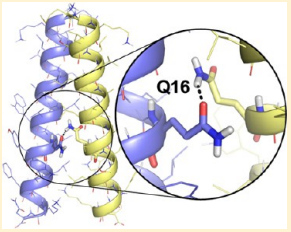

Cell division is one of the most fundamental processes in the life of bacteria. In Gram-negative bacteria, division requires a complex and coordinated remodeling of the three-layer cell envelope, and therefore mechanisms must exist to sort the duplicated chromosome, to provide constrictive force, to synthesize the septal cell wall, and, finally, to induce membrane fusion. These events are enabled by a multiprotein complex called the divisome. The assembly of the divisome begins with the formation of a ring-like structure at the site of division (the Z-ring), where the polymeric FtsZ likely provides constrictive force and forms a scaffold for the recruitment of the complex.[1−3] In *Escherichia coli* the recruitment of the essential proteins follows a strikingly linear hierarchy, illustrated in Figure 1a.[4] The cytoplasmic side of the ring is formed by the early components: FtsA, a membrane-associated actin family member that forms protofilaments;[5,6] ZipA, a single-pass membrane protein that contributes to FtsZ tethering along with FtsA;[7,8] and FtsK, a DNA translocase that is essential for unlinking chromosome dimers after homologous recombination.[9] In contrast, the late proteins perform functions related to the reconstruction of the cell-wall: FtsW is a transporter of cell-wall precursors across the membrane;[10,11] FtsI is important for the cross-linking of the cell wall during division;[12] and FtsN is necessary for the recruitment of nonessential septal components, the murein hydrolase AmiC,[13,14] and the Tol-Pal complex required for proper invagination during constriction.[15]

The early and late components of the divisome are linked by a trio of single pass transmembrane (TM) proteins: FtsQ, FtsB, and FtsL. The ability of FtsB and FtsL to recruit the late

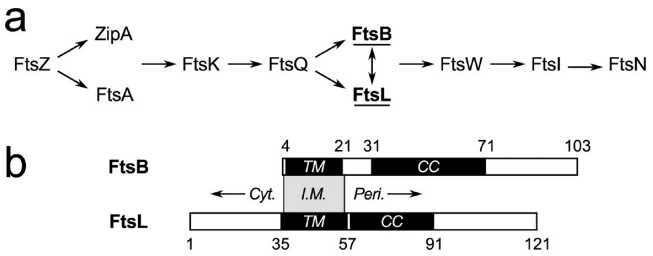

Figure 1. The recruitment hierarchy of the divisome and the predicted topology of FtsB and FtsL. (a) In *E. coli* the recruitment of the divisome to the division site follows a strict hierarchical dependency.[4] A functional FtsZ is required for the recruitment of FtsA and ZipA, which in turn are required for the recruitment of FtsK, and so on. FtsB and FtsL are codependent for their recruitment and both depend on FtsQ. (b) Putative domain topology of FtsB and FtsL, as annotated in UniProt. Their interaction is presumed to be mediated by their single transmembrane domain (TM) and a juxta-membrane coiled coil region (CC). The start and end positions of the predicted TM and CC domains are indicated. Cyt. = cytoplasm. I.M. = inner membrane. Peri. = periplasm.

divisome elements suggests that they have a structural role as a scaffold in the assembly of the divisome,[16] and it has been proposed that they are involved in Z-ring stabilization.[17] FtsB and FtsL may also be involved in a regulatory checkpoint of

Received: February 20, 2013
Revised: March 22, 2013
Published: March 22, 2013

division because the depletion of FtsB from *E. coli* cells results in the disappearance of FtsL.[18] The cellular instability of FtsL was also observed in *Bacillus subtilis*,[19−21] where $FtsL_B$ is rapidly degraded by the intramembrane protease RasP unless it is stabilized by its interaction with the FtsB homologue (DivIC).[22] These observations led to an unconfirmed hypothesis that active proteolysis of FtsL may be a regulatory factor in the timing of bacterial cell division.[23]

While the precise function of FtsB and FtsL is not well understood, substantial evidence indicates that they physically interact with each other. As highlighted in Figure 1a, FtsB and FtsL are mutually dependent for their recruitment at the division site, and both proteins depend on the localization of FtsQ.[18,24] A similar picture has been reported in *B. subtilis*, where the localization of the homologues of $FtsL_B$ and DivIC depends on the FtsQ homologue (DivIB) at the temperature at which DivIB is essential.[20,25] There is strong evidence that FtsB and FtsL form a stable subcomplex *in vivo*. A complex comprising FtsB, FtsL, and FtsQ was isolated from *E. coli* by coimmunoprecipitation.[26] The physical interaction of the *E. coli* and *B. subtilis* proteins was also confirmed by two-hybrid analysis.[21,27,28] Further evidence of a stable interaction between FtsB and FtsL was obtained with a series of artificial septal targeting experiments[16,29−33] that demonstrated that FtsL and FtsB interact with each other and can recruit the downstream proteins even when FtsQ has been depleted from the cell.[30] Moreover, the *B. subtilis* homologues $FtsL_B$ and DivIC form a complex when coexpressed in *E. coli* despite the fact that they are unlikely to interact with the significantly divergent *E. coli* division proteins.[31]

The domain organization of FtsB and FtsL (Figure 1b) suggests that they may interact through an extended helical structure encompassing the membrane and periplasmic regions. Both proteins contain a TM domain and a juxta-membrane coiled coil, in addition to a small (FtsL) or minimimal (FtsB) cytoplasimic N-terminal tail. The TM and coiled coil regions of FtsB are necessary and sufficient for its interaction with FtsL,[16] and similarly, the TM and coiled coil regions of FtsL are both essential for its interaction with FtsB.[26] A low resolution model of the soluble domains of the *Streptococcus pneumoniae* homologues of FtsB, FtsL, and FtsQ was proposed by Masson et al.,[34] based on a combination of NMR, small angle neutron, and X-ray scattering, and surface plasmon resonance. In this study the TM domains were truncated and replaced by a soluble coiled coil pair.[34,35] More recently, a bioinformatic analysis of the soluble domains of FtsB, FtsL, and FtsQ suggested two alternative models with 1:1:1 or 2:2:2 oligomeric stoichiometries.[36] However, no structural information was available regarding the organization of the important TM region.

In an effort toward understanding the structural organization and precise oligomeric state of the FtsB-FtsL complex, we investigated the self-association propensities of both TM and soluble regions of the two individual proteins. We hypothesized that if the FtsB-FtsL complex is larger than a dimer, one or both proteins could potentially self-associate and be studied in isolation. Indeed, we found that FtsB homo-oligomerizes. Here we present a structural analysis obtained with a combination of extensive mutagenesis, computational modeling, and X-ray crystallography. The results provide a theoretical scaffold for the biophysical characterization of the FtsB−FtsL heterologous complex and offer several structure-based hypotheses that can be tested in the context of cell division by functional studies *in vivo*.

MATERIALS AND METHODS

Vectors and Strains. All oligonucleotides were purchased in desalted form from Integrated DNA Technologies and used without purification. The expression vectors pccKAN, pccGpA-wt, and pccGpA-G83I, and *malE* deficient *E.a coli* strain MM39 were kindly provided by Dr. Donald M. Engelman.[37] Genes encoding the TM domains of FtsB and FtsL were cloned into the NheI-BamHI restriction sites of the pccKAN vector resulting in the following protein sequences: FtsB "...NRASLALTLLLLAILVWLQYSLWFGILIN..."; FtsL "...NRASFGKLPLCLFICIILTAVTVVTTAGILIN...". All mutagenesis was done with the QuikChange kit (Stratagene).

The periplasmic segment of FtsB was obtained from the *E. coli* genome (K12 strain) by PCR using PfuUltra II Fusion DNA polymerases (Stratagene) and cloned into a pET31b vector containing the fusion protein Gp7, using a modified QuikChange protocol that includes the use of PfuUltra II Fusion DNA polymerase, 1 min annealing time, 2 min/kb extension time at 65 °C, 50 ng of template, and 100−150 ng of the first round PCR product, in the presence of 4% DMSO.[38] All constructs generated throughout the studies were sequence-verified over the entire ORF insert and at least 50 bp upstream and downstream of the ORF. The resulting plasmids containing Gp7-FtsB fusions were transformed into BL21-DE3 cells for overexpression and further analyses.

Expression of Chimeric Proteins in MM39 Cells and MalE Complementation Assay. The TOXCAT constructs were transformed into MM39 cells. A freshly streaked colony was inoculated into 3 mL of LB broth containing 100 μg/mL ampicillin and grown overnight at 37 °C. Overnight cultures were inoculated into 3 mL of LB broth at a ratio of 1:1000 and grown to an OD_{420} of approximately 1 (OD_{600} of 0.6) at 37 °C. After recording of the optical density, 1 mL of cells was spun down for 10 min at 17000*g* and resuspended in 500 mL of sonication buffer (25 mM Tris-HCl, 2 mM EDTA, pH 8.0). Cells were lysed by probe sonication at medium power for 10 s over ice, and an aliquot of 50 μL was removed from each sample and stored in SDS-PAGE loading buffer for immunoblotting. The lysates were then cleared by centrifugation, and the supernatant was kept on ice for chloramphenicol acetyltransferase (CAT) activity assay. To confirm for proper membrane insertion of the TOXCAT constructs, overnight cultures were plated on M9 minimal medium plates containing 0.4% maltose as the only carbon source and grown at 37 °C for 48 h.[37] The variants that did not grow in these conditions were not considered in the study.

Chloramphenicol Acetyltransferase (CAT) Spectrophotometric Assay. CAT activity was measured as described.[39,40] One milliliter of buffer containing 0.1 mM acetyl coA, 0.4 mg/mL 5,5′-dithiobis-(2-nitrobenzoic acid), and 0.1 M Tris-HCl pH 7.8 was mixed with 40 μL of cleared cell lysates, and the absorbance at 412 nm was measured for 2 min to establish the basal activity rate. After addition of 40 μL of 2.5 mM chloramphenicol in 10% ethanol, the absorbance was measured for an additional 2 min to determine CAT activity. The basal CAT activity was subtracted, and the value was normalized by the cell density measured as OD_{420}. All measurements were determined at least in duplicate, and the experiments were repeated at least twice.

dx.doi.org/10.1021/bi400222r | *Biochemistry* 2013, 52, 2574−2585

Quantification of Expression by Immunoblotting. Protein expression was confirmed by immunoblotting. The cell lysates (10 μL) were loaded onto a NuPAGE 4−12% Bis-Tris SDS-PAGE gel (Invitrogen) and then transferred to PVDF membranes (VWR) for 1 h at 100 millivolts. Blots were blocked using 5% bovine serum albumin (US Biologicals) in TBS-Tween buffer (50 mM Tris, 150 mM NaCl, 0.05% Tween 20) for 2 h at 4 °C, incubated with biotinylated anti-maltose binding protein antibodies (Vector laboratories), followed by peroxidase-conjugated streptavidin (Jackson ImmunoResearch). Blots were developed with the Pierce ECL Western Blotting Substrate Kit, and chemiluminescence was measured using an ImageQuant LAS 4000 (GE Healthsciences).

Expression of Chimeric Proteins in BL21-DE3 Cells for *E. coli* Overexpression and Ni-NTA Purification. The Gp7-FtsB chimerae, with an added C-terminal six-His tag preceded by the recognition site for TEV protease, were expressed in *E. coli* BL21-DE3 cells using a modified pET31b vector. A single colony was grown at 37 °C in 50 mL overnight and then inoculated into 4L of LB broth. Cells were grown to an OD_{600} of 0.8−1.0 before addition of 1 mM IPTG to induce overexpression which was carried out for 18 h at 18 °C. The cell pellets were washed and stored at −80 °C until purification. All Gp7 fusion proteins were purified using an identical protocol. Typically, 8−12 g of frozen cell pellets were mixed with 10 mL of lysis buffer (50 mM NaCl, 5 mM β-mercaptoethanol, 0.5 mg/mL lysozyme, 50 mM HEPES pH 8.0, 1 mM phenylmethylsulfonyl fluoride) per gram of cell pellet and lysed by sonication. Lysates were cleared using centrifugation at 45000*g* for 30 min (JA 25.5 rotor). Cleared lysates were loaded onto 5 mL of Ni-NTA resin, washed extensively with Buffer A (300 mM NaCl, 1 mM β-mercaptoethanol, 20 mM imidazole, 25 mM HEPES, pH 8.0), and eluted with Buffer B (same as Buffer A, but with 300 mM imidazole). The eluted fractions were mixed with TEV protease at a molar ratio of ∼1:40 and dialyzed at 4 °C overnight against Buffer C (10 mM HEPES, 100 mM NaCl, 0.5 mM TCEP, 0.1 mM EDTA pH 8.0). The TEV protease was prepared as described.[41] The dialysate was repurified on Ni-NTA, this time by collecting fractions that elute during washes with lower imidazole (Buffer A). The pure fractions were pooled and dialyzed against Buffer C again and concentrated to ∼10 mg/mL using an Ultracel-10K (Millipore), clarified by centrifugation at 5000*g*, and finally flash frozen as 30 μL droplets in liquid nitrogen and stored at −80 °C.

Circular Dichroism (CD). The purified Gp7-FtsB constructs were diluted to 0.2−0.4 mg/mL for CD analysis. CD measurements were carried out on an Aviv 202SF spectropolarimeter. Samples were measured in 1 mM Hepes pH 8, 10 mM NaCl, and 0.1 mM TCEP. The thermostability studies were performed under the same buffer conditions with a temperature ramp of 3 °C/min, and the ellipticity was monitored at 222 and 208 nm.

Crystallization of Gp7-FstB. Gp7-FtsB was screened for initial crystallization conditions by vapor diffusion at 20 °C with a 144-condition sparse matrix screen developed in the Rayment laboratory. Crystals of Gp7-FtsB were grown by vapor diffusion at 20 °C from a 1:1 (v/v) mixture of protein at 10 mg/mL with 100 mM Bis-Tris, 5 mM gamma-caprolactone, 2.1 M ammonium sulfate, 0.6 M malonate, 5% glycerol, pH 6.5. After one day hexagonal crystals measuring 0.1 × 0.1 × 0.5 mm were observed. The crystals were soaked in mother liquor for 24 h subsequent to flash freezing in liquid nitrogen. Gp7-FtsB crystallized in the space group $P6_1$ with unit cell dimensions of a = 87.6 Å, b = 87.6 Å, and c = 185.1 Å where two Gp7-FtsB dimers were present in the asymmetric unit.

Data Collection and Structure Determination for Gp7-FtsB. X-ray data for Gp7-FtsB were collected at 100 K on the Structural Biology Center beamline 19ID at the Advanced Photon Source in Argonne, IL. Diffraction data were integrated and scaled with HKL3000.[42] Data collection statistics are given in Supplementary Table S1. A molecular replacement solution was obtained using residues 2−48 of Gp7 (PDB entry 1NO4)[43] as a search model in the program Molrep.[44] The electron density was improved with the program Parrot and the initial model was built using Buccaneer.[45,46] Final models were generated with alternate cycles of manual model building and least-squares refinements using the programs Coot[47] and Refmac.[48] Refinement statistics are presented in Supplementary Table S1.

Computational Modeling. The TM oligomer of FtsB was modeled with programs written in house and distributed with the MSL molecular modeling libraries v. 1.1,[49] available at at http://msl-libraries.org. The *predictHelixOligomer* program creates standard helices and performs a global rigid search altering the interhelical separation, the crossing angle, the crossing point, and the axial orientation of the helices. To impose the formation of an interhelical hydrogen bond involving Gln 16, the conformational space was prescreened prior to the analysis to exclude the region of space that was incompatible with the program *filterOligomerByConstraint*. This was performed on helices in which all amino acids were converted to Ala except Gln 16, Tyr 17, and Ser 18. The backbone was kept rigid during the procedure, while the side chains were optimized using a greedy trials method implemented in MSL.[49,50] Side chain mobility was modeled using the Energy-Based conformer library applied at the 90% level.[51] The models were evaluated using a van der Waals function with CHARMM 22 parameters and the SCWRL hydrogen bond function implemented in MSL. The models were sorted by their energies. All low-energy models were visually inspected to verify that they did not include poorly packed solutions containing cavities. The computational mutagenesis was performed on all low-energy models by applying the same mutation studied experimentally in the context of a fixed backbone, followed by side chain optimization. The relative energy of each mutant was calculated as

$$\Delta E_{\mathrm{mut}} = (E_{\mathrm{mut,dimer}} - E_{\mathrm{mut,monomer}}) - (E_{\mathrm{WT,dimer}} - E_{\mathrm{WT,monomer}})$$

where $E_{\mathrm{WT,dimer}}$ and $E_{\mathrm{mut,dimer}}$ are the energies of the wild type and mutant sequence in the dimeric state, and $E_{\mathrm{WT,monomer}}$ and $E_{\mathrm{mut,monomer}}$ are the energies of the wild type and mutant sequence in a side chain optimized monomeric state with the same sequence. The effect of each mutation was classified in four categories analogously to the experimental mutagenesis using the following criterion: category 0, "WT-like", $\Delta E_{\mathrm{mut}} < 2$ kcal/mol; category 1, "Mild", $2 \leq \Delta E_{\mathrm{mut}} < 4$; category 2, "Severe", $4 \leq \Delta E_{\mathrm{mut}} < 8$; category 3, "Disruptive", $\Delta E_{\mathrm{mut}} \geq 8$. The numerical category values were averaged to calculate the position dependent average disruption value reported in Figure 5.

Creation of TM + Coiled Coil Model. The computational model of the TM domain and the coiled coil region were

connected together using fragments from the PDB database. To do this, protein fragments of the pattern *hhx*G*xx*G*xhh* (where *x* is any amino acid, and *h* is any amino acid in a helical conformation) were extracted from high resolution X-ray structures deposited in the PDB database with a resolution of 2 Å or better. The MSL program *connectWithFragments* takes these fragments and aligns the helical end residues with the corresponding residues in the coiled coil domain and then the modeled TM domain. Only the N, C, CA, and O atoms were considered for the alignment and the fragments with the lowest R.M.S.D. were selected. The side chains on the fragment were replaced with the one corresponding to the FtsB sequence and their conformation was optimized using a greedy trials method.

FtsB Sequence Alignment and Consensus Sequence. The alignment was obtained by entering the sequence of *E. coli* FtsB as the query in BLAST (http://blast.ncbi.nlm.nih.gov) using the blastp algorithm with default settings. The resulting 464 sequences were aligned with the multiple alignment facility in BLAST (COBALT). The prevalent amino acid at each position in the sequence was used to determine a consensus sequence if it was present in at least 30% of the sequences.

Accession Numbers. Coordinates and structure factors of Gp7-FtsB have been deposited in the Protein Data Bank with PDB ID code 4IFF.

RESULTS AND DISCUSSION

The Transmembrane Domain of FtsB Self-Associates. To determine if the TM domains of FtsB and FtsL from *E. coli* self-associate, we analyzed them with TOXCAT, a widely used biological assay for TM association.[37] The assay is based on a chimeric construct in which the TM domain of interest is fused to the ToxR transcriptional activator domain from *Vibrio cholera* (Figure 2a). Oligomerization, driven by the TM helices, results in the expression of the reporter gene chloramphenicol acetyltransferase (CAT). The expression level of CAT (measured enzymatically) is compared to that of a stable dimer, glycophorin A (GpA), as a standard. While TOXCAT is applicable to membrane proteins of any origin (GpA for example is a human protein), it is significant that in the case of FtsB and FtsL the analysis is performed in their native *E. coli* membrane. This fact also raised an initial concern that the TOXCAT constructs could potentially interfere with the cell division process. Fortunately, this concern was unfounded as the cells grew and divided normally.

The results of the TOXCAT analysis of FtsB and FtsL are shown in Figure 2b. The CAT activity of both constructs is above background, although the association of FtsL appears to be weak (19% of the GpA signal). The activity of FtsB is approximately half of the GpA signal (48%), indicating that the homo-oligomerization of its TM domain is likely stable.

The Transmembrane Self-Association of FtsB Is Mediated by a Critical Polar Amino Acid. To investigate what amino acids are important for the self-association of FtsB and FtsL, we systematically mutated each position and monitored the effects on association. The expectation is that the changes at interfacial positions would perturb oligomerization more than the changes at positions that are lipid exposed, as commonly observed (for example[52−56]). We applied an initial scanning mutation strategy using both Ala (small) and Ile (large) substitutions and then expanded the mutagenesis to include a larger variety of hydrophobic amino acids.

Figure 3 shows the TOXCAT data for the 57 single amino acid variants tested for FtsB. All variants displayed similar levels

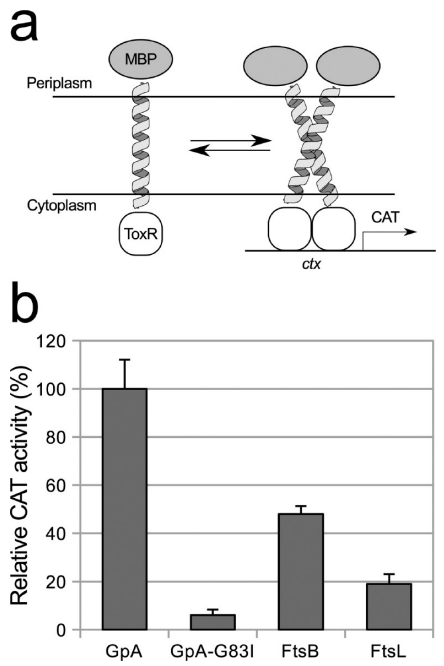

Figure 2. FtsB self-associates in TOXCAT. (a) TOXCAT is an *in vivo* assay based on a construct in which the transmembrane domain under investigation is fused to the ToxR transcriptional activator of *V. cholerae*. Transmembrane association results in the expression of a reporter gene in *E. coli* cells, which can be quantified. (b) TOXCAT assay of FtsB and FtsL transmembrane domains. FtsB shows half of the activity of the strong transmembrane dimer of glycophorin A (GpA). The activity of FtsL is above baseline but low, indicating a weak propensity to homo-oligomerize. The monomeric G83I mutant of GpA is used as a negative control. Data are reported as average and standard deviation over four replicate experiments.

of TOXCAT construct expression, as verified by Western blot analysis (data not shown). While a majority of the variants have a CAT activity level comparable to the wild type constructs, there are a number of mutations that display drastically reduced activity. Conversely, several constructs with significantly increased activity were also observed. To obtain an estimate of the overall sensitivity of each position, we applied a simple classification scheme for the variants' phenotypes using four categories (dashed lines in Figure 3), labeled as "WT-like" (>80% of wild type CAT activity), "Mild" (50−80%), "Severe" (20−50%), and "Disruptive" (0−20%). We then averaged the scores to obtain a position specific disruption index. Position-based averaging reduces some of the natural variability of the biological assay, and the method has been reliable in identifying the most sensitive positions at the helix−helix binding interface.[52,56,57] The classification data is schematically represented in Figure 4a.

When the average disruption is projected on a helical wheel diagram (Figure 4b), it becomes evident that the sensitive mutations cluster on one helical face defined by positions T5, L6, L8, L9, L12, L15, Q16, L19, and W20. When the average disruption is fit to a sine function to analyze its periodicity (Figure 4c), we obtained a value of 3.5 amino acids per turn, which suggests that the helices of the FtsB oligomer interact with a left-handed crossing angle. Interestingly, the variants with enhanced CAT activity (A10, W14, Y17, W20, and F21) are primarily located on the opposite face relative to the disruptive positions. Therefore, it seems unlikely that these

dx.doi.org/10.1021/bi400222r | *Biochemistry* 2013, 52, 2574−2585

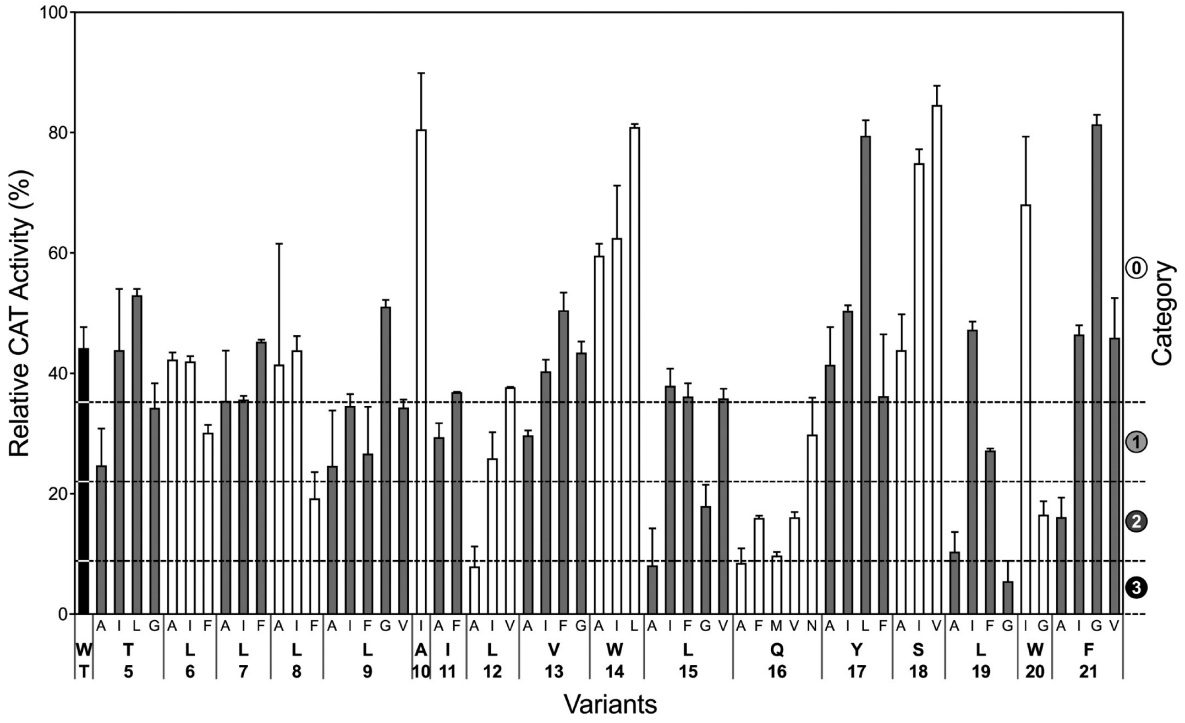

Figure 3. Mutagenesis of the transmembrane helix of FtsB. The figure shows the 57 point mutants of the TM domain of FtsB (residues 5−21) analyzed in TOXCAT. The CAT activity (left axis) is normalized to that of the GpA construct, as in Figure 2. The activity of the wild type FtsB construct is in black. The mutations at each position are visually grouped by color. Each mutation has been categorized relative to the wild type FtsB TOXCAT activity (back bar) as "WT-like" (0: >80% of WT), "Mild" (1: 50−80%), "Severe" (2: 20−50%), or "Disruptive" (3: 0−20%), as indicated on the right axis and by the dashed lines. The TOXCAT data for all 57 variants is summarized using the above category scheme in Figure 4.

variants enhance stability by direct participation to the interaction interface.

We attempted a similar mutagenesis analysis for FtsL. While a number of mutations that appear to be disruptive were identified, the disruption pattern does not clearly map to a helical interface as in the case of FtsB, indicating that that the weak self-association of FtsL observed in TOXCAT is unlikely to be specific in nature.

FtsB Self-Association Is Mediated by Interhelical Hydrogen Bonding. Among the positions of the TM domain of FtsB that are sensitive to mutation, Gln 16 is of particular interest. Polar amino acids, such as Gln, Asn, Glu, Asp, Lys, Arg, and His, are not frequent in TM domains, which are primarily composed by hydrophobic residues.[58,59] When present, however, polar residues can stabilize the association of TM helices through the formation of hydrogen bonds, which are enhanced in an apolar environment.[60,61] While the energetic contribution of hydrogen bonding to membrane protein folding appears to be on average rather modest (∼1 kcal/mol),[61,62] polar amino acids can be important for the association of model peptides[63,64] and of biological systems.[40,65−68] When present, polar amino acids are also likely to play an important structural or functional role, and it has been observed that phenotypic alterations and diseases are likely to result from mutations that reverse the polarity of an amino acid in membrane proteins.[69,70]

When Gln 16 is substituted by hydrophobic amino acids (Ala, Phe, and Val), the oligomerization of FtsB appears to be severely reduced (Figures 3 and 4). Even when the Gln was replaced by a nonpolar amino acid with similar size and flexibility (Met) the CAT activity decreased to 22% of WT. Conversely, when position 16 is substituted by Asn, which has the same amide terminal moiety of Gln, the variant retains most of the activity (67%). This result confirms that hydrogen bond formation is likely to play a major role in stabilizing the TM oligomer. Two side chains that could potentially hydrogen bond with Gln 16 across the interface are Tyr 17 and Ser 18. However, the removal of their hydroxyl groups (Y17F and S18A variants) did not appear to reduce oligomerization. This observation suggests that Gln 16 is likely to donate to a carbonyl oxygen atom from the backbone or to form a hydrogen bond with itself (from the opposing helix), a hypothesis that we structurally investigated using computational modeling, as presented in the next section.

Computational Model of a FtsB Left-Handed Homodimer. Molecular modeling can interpret the wealth of information contained in large-scale mutagenesis and synthesize it into an often highly accurate structural hypothesis.[52−54,71] The modeling of the TM domain of FtsB was performed with a search protocol implemented with the molecular software library developed in this laboratory (MSL).[49] The program generates helices in standard conformation and systematically varies their relative orientation to explore conformational space. In this calculation, we imposed the formation of a symmetrical oligomer. Consistently with the experimental data, we also required that Gln 16 forms an interhelical hydrogen bond in the structure. The calculation produced two well packed dimeric low-energy solutions (Figure 5). In one solution (Model 1, panel a), Gln 16 is hydrogen bonded nonsymmetrically with Gln 16 on the opposite side. In Model 2 (panel b), the side chain is hydrogen bonded symmetrically to the carbonyl oxygen of Val 13. The two models are closely related (1.5 Å RMSD), having a similar left-handed crossing angle and interhelical distance, and differing by a relative rotation of

dx.doi.org/10.1021/bi400222r | Biochemistry 2013, 52, 2574−2585

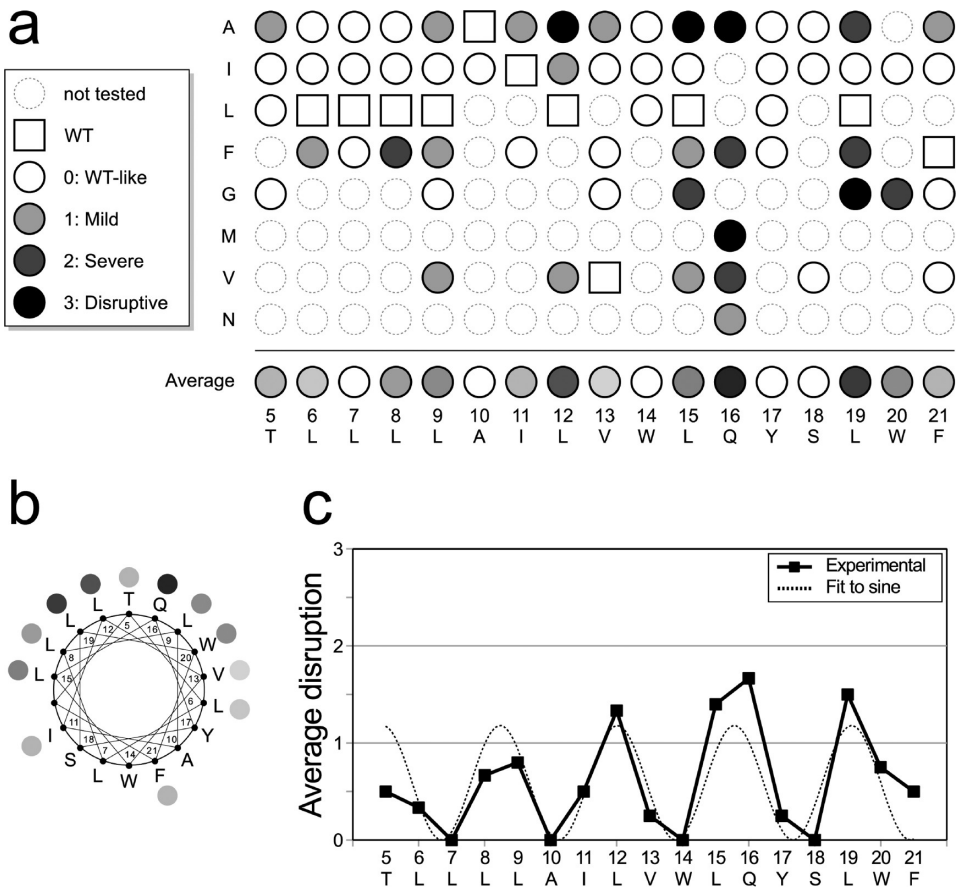

Figure 4. Position specific "average disruption" identifies a helical interface and an essential polar residue. (a) The scheme summarizes the effect of all mutations of FtsB-TM measured in TOXCAT. The data have been categorized as explained in Figure 2. An average disruption score is displayed at the bottom of the scheme. While Gln 16 is the most sensitive position, the introduction of an Asn side chain restores association almost entirely, indicating that a hydrogen bond is important for the association. (b) Diagram mapping the average disruption score to a helical wheel. The disruption pattern clusters on one helical face defined by positions T5, L6, L8, L9, L12, L15, Q16, L19 and W20. (c) Fit of the average disruption index to a sine function. The estimated periodicity is approximately 3.5 amino acid per turn, which corresponds to a helical interaction with a left-handed crossing angle (dotted line).

approximately 60° applied around the helical axis. To identify which solution was most compatible with the experimental data, we applied *in silico* the same set of mutations that were experimentally tested and computed an analogous average disruption. The theoretical and experimental disruption patterns are compared in Figure 5c,d. Model 2 is in reasonable agreement with the data overall, but its periodicity appears be slightly off-phase with respect to the experimental data, and the match becomes poor toward the C-terminal end of the helix (panel d). Model 1 (panel c) is in excellent agreement with the experimental data, and therefore we propose it as the most likely structural interpretation. Model 1 is illustrated in more detail in Figure 6 where the specific orientation of the side chains at the dimer interface is shown and the contacts are described. A PDB file of the two models can be found as Supporting Information and downloaded from http://seneslab.org/FtsBdimer.

Gln 16 and the Interfacial Amino Acids of the Transmembrane Domain of FtsB Are Evolutionarily Conserved. To investigate if the interfacial amino acids, and Gln 16 in particular, are evolutionarily important, we performed a multisequence alignment of related FtsB sequences obtained using BLAST[72,73] and computed a consensus. A condensed version of the alignment is shown in Figure 7, and the complete analysis of all 464 sequences is provided as Supporting Information (Figure S1). The TM region of FtsB appears to be relatively well conserved across a broad group of gamma and beta proteobacteria. Most importantly, the pattern of conservation (shaded columns) corresponds remarkably well to the positions that have the highest sensitivity to mutagenesis (indicated by a dot). The average amino acid identity conservation of the sensitive positions is 68%, compared to 42% of the other positions. The most conserved positions is Trp 20, which is found in over 95% of the sequences. The key Gln 16 is also almost invariable (91% of the sequences). Interestingly, its most frequent substitution is His (4%), another polar amino acid. These observation supports the hypothesis that the structural organization of the TM domain of FtsB is evolutionarily conserved and therefore must be of biological importance for cell division.

The X-ray Crystal Structure of the Periplasmic Region of FtsB Reveals a Canonical Coiled Coil. After determining the organization of the TM domain of FtsB, we were interested in establishing if the periplasmic coiled coil region is also compatible with the formation of a homodimer. We approached this question by using X-ray crystallography. Unlike TM helices, which are stabilized by the hydrophobic environment, the soluble coiled coils tend to be unstable in isolation.[34] For this reason we adopted a fusion strategy, replacing the TM region with a soluble globular protein

dx.doi.org/10.1021/bi400222r | *Biochemistry* 2013, 52, 2574−2585

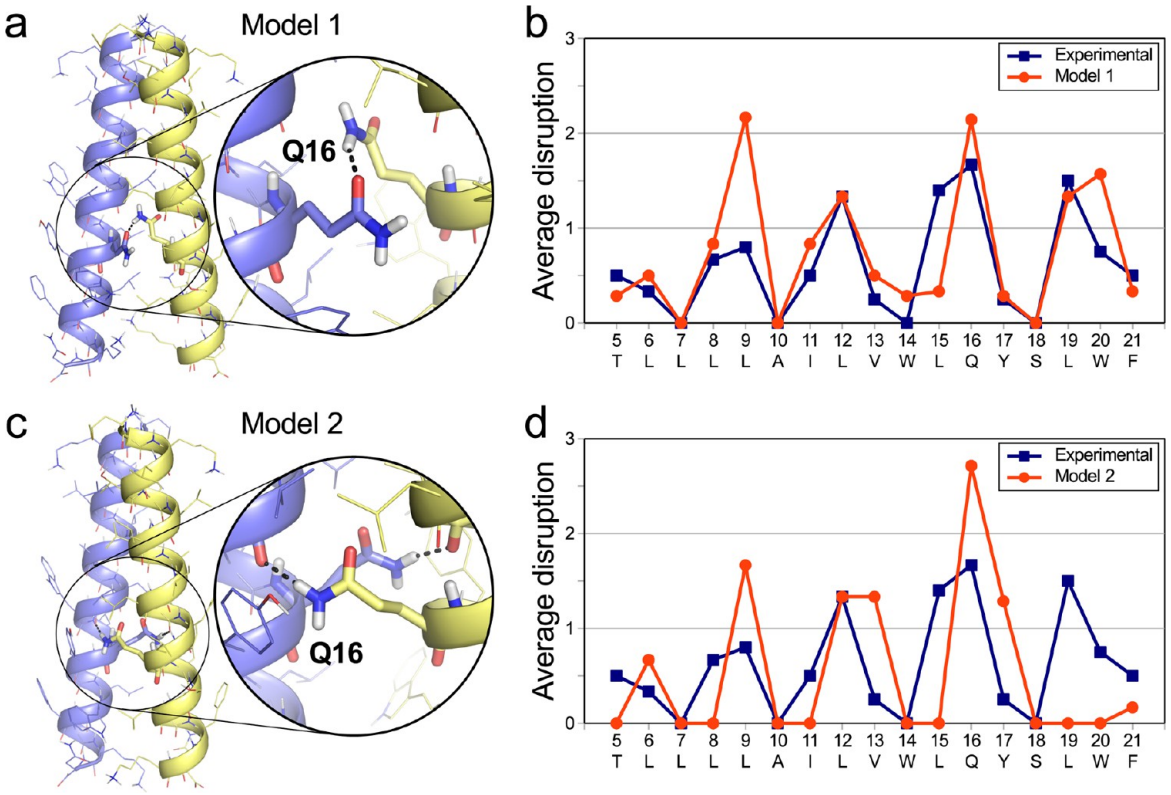

Figure 5. Molecular model of the FtsB transmembrane dimer. Modeling identified two well packed low-energy structures in which Gln 16 forms an interhelical hydrogen bond (panels a and c). Models 1 and 2 are closely related (Cα RMSD of 1.5 Å), with a left-handed crossing angle (25° and 20°, respectively) and an interhelical distance of 10.1 Å. In Model 1 the side chains of Gln 16 interact with a nonsymmetrical hydrogen bond. The helices of Model 2 are rotated axially by about 60° with respect to Model 1. The side chains of Gln 16 interact symmetically with the carbonyl oxygen of Val 13. Panels b and d compare the average disruption index for the computational mutagenesis applied to the models to the average disruption observed experimentally. Model 1 shows an excellent agreement with the experimental data, which is better than Model 2, particularly in the C-terminal side of the transmembrane domain.

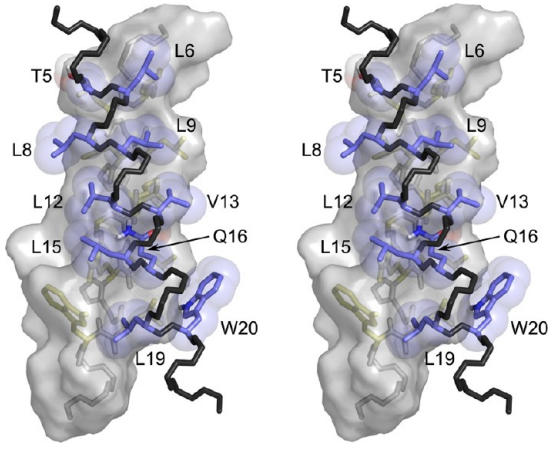

Figure 6. Computational model of FtsB-TM (Model 1). Stereo representation of the side chain interactions across the interface. The interacting positions on the opposite chains are shown in sticks to highlight the arrangement and packing of the side chains. The van der Waals sphere of the side chains of the monomer in the foreground (blue) and the surface of the monomer in the background are also displayed with transparency. L15 and L19 interact against a ridge formed by W20. L12 and V13 pack against each other across the interface, and so do the L8/L9 and the T5/L6 pairs.

(bacteriophange Φ29 Gp7) which nucleates the helix and stabilizes the coiled coil. This strategy has been demonstrated to greatly improve the solubility and crystallization propensity of coiled coil domains.[74,75]

A Gp7 fusion construct encompassing amino acids 28−63 of FtsB (Gp7-FtsB$_{CC}$) crystallized readily, and its structure was solved at a 2.3 Å, with two dimeric molecules in the asymmetric unit (Supplementary Figure S2a). The X-ray data collection and refinement statistics are provided in Supplementary Table S1. The structure of the Gp7-FtsB$_{CC}$ dimer is shown in Figure 8, where the Gp7 moiety is highlighted in gray and the FtsB component in blue. This region of FtsB adopts a canonical coiled coil conformation. As expected, the two Asn residues that are present at "*a*" heptad positions (Asn 43 and 50) form a hydrogen bond across the interface with their corresponding residues on the other chain (Figure 8b). The coil is straight for one of the dimers (chains A-B), but it exhibits a slight kink in the second (near Val 36 on chain C−D, supplementary Figure S2b). The overall RMSD between the two dimers is 1.74 Å, but it decreases to 0.41 Å and 0.81 Å when the pre- and postkink segments are aligned separately; therefore, the kink is presumably due to the effect of crystal packing.

The structure demonstrates that, like the TM domain, the coiled coil region of FtsB can also assume a homodimeric form. The structure also determines that the coiled coil region of FtsB can extend at least to position 60. It is not clear whether the coiled coil would extend further, at least in the absence of FtsL. Gonzales and Beckwith determined that a C-terminal truncation of FtsB starting position 55 is still sufficient to interact with FtsL.[16] Circular dichroism (CD) analysis of a

dx.doi.org/10.1021/bi400222r | *Biochemistry* 2013, 52, 2574−2585

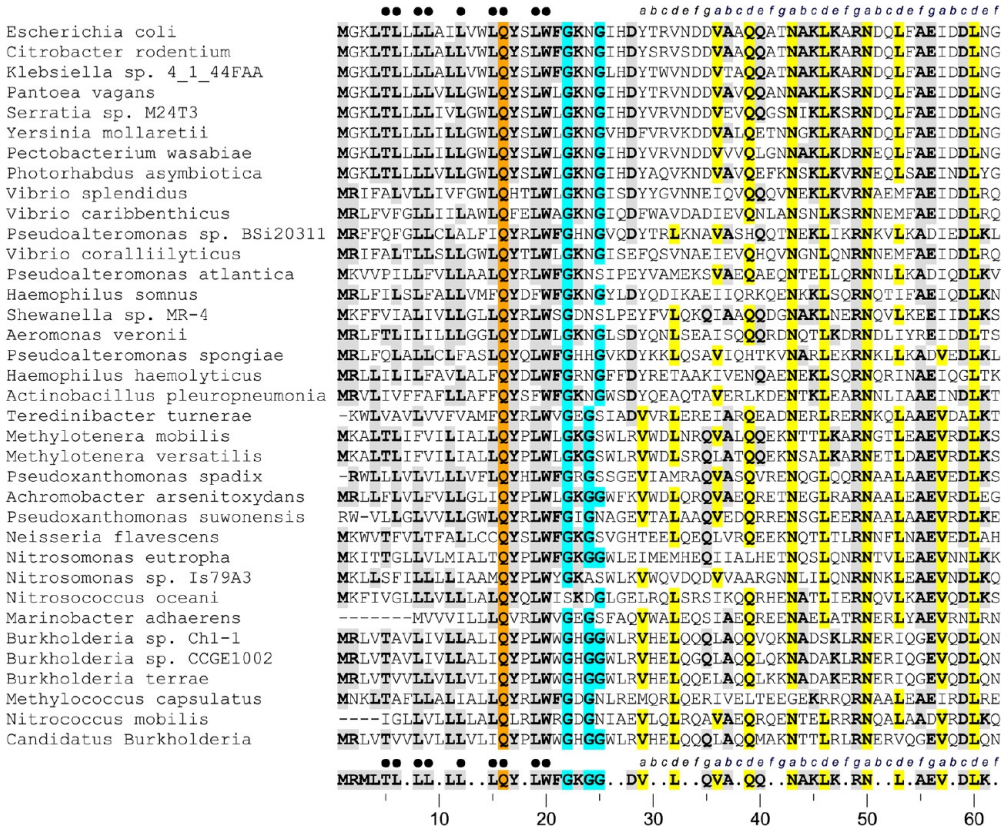

Figure 7. Sequence alignment of FtsB indicates that the interfacial positions are evolutionary conserved. Partial representation of a sequence alignment of FtsB. The complete alignment is provided in Supplementary Figure S1. FtsB is relatively well conserved among a diverse group of beta and gamma proteobacteria. The amino acids that are present in at least 30% of sequence at each position are shown in bold and shaded. These amino acids are also highlighted in the consensus sequence at the bottom of the alignment. The positions that are involved at the FtsB dimer interface (Figure 5) are marked with a full circle (●). A remarkable match between conservation and the interfacial positions is evident. In particular, positions Q16 (highlighted in orange), L20 and W21 are almost invariable. The heptad repeat designation (positions *a* to *g*) of the coiled coil region is also given, and the conserved amino acids at the interfacial *a* and *d* positions are highlighted in yellow. In cyan are highlighted three conserved Gly amino acids (positions 22, 24, and 25) that are likely to confer flexibility to the linker region between the transmembrane domain and the coiled coil region.

longer constructs that encompassed seven heptad repeats (positions 28−77) revealed that it is poorly helical (Supplementary Figure S3). A Gp7-FtsB$_{CC}$ construct that contains the entire soluble region of FtsB is also only moderately helical.

Flexibility May Be Important between the Transmembrane and Coiled Coil Region of FtsB. There is a gap of six amino acids (positions 22−27) between the computational model of the TM domain and the X-ray structural model of the periplasmic coiled coil, raising the question of how these two regions are connected. The simplest hypothesis would be that the two domains form a seamless helical structure that transverses the TM region and extends into the periplasm. Our geometric analysis, however, revealed that the two models cannot be connected by a simple fusion of their helices. While the crossing angle and interhelical distance of the two domains match each other, the orientation of the helices around their main axes is not compatible. The interface of the TM region is rotated around the helical axis by approximately 100° with respect to the interface that would result from a natural extension of the coiled coil.

The analysis of the sequence alignment (Figure 7) also supports the hypothesis that a helical break is likely present in the linker region between the domains. The alignment reveals that two Gly residues at positions 22 and 25 are highly conserved (highlighted cyan). Gly 22 is present in 93% of the sequences. Gly 25 is less ubiquitous (63% of the sequences), but a third Gly is frequently present at position 24 (47%). Interestingly, the other amino acids that are prevalent at positions 24 and 25 are Ser and Asn, two residues that have a relatively high propensity for random-coil regions.[76] The data suggest that the linker requires either flexibility or adopts a backbone conformation that would be inaccessible to non-Gly amino acids, or perhaps both. According to this view, we mined the structural database for protein fragments that contained two Gly residues with the correct spacing (G*xx*G) to find candidate linkers for the two models. We extracted all *x*G*xx*G*x* fragments existing in high-resolution structures from the PDB, where *x* is any amino acid. We also imposed a constraint that two additional residues at each side of the fragment must assume a helical conformation (thus the pattern becomes *hhx*G*xx*G*xhh*, where *h* is any amino acid in helical conformation). These helical amino acids were geometrically aligned with the ends of the TM and coiled coil structure. With this procedure, we were able to identify the low-energy solution that connects the two models illustrated in Figure 9.

Is FtsL Required to Stabilize the Periplasmic Domain of FtsB? While the model of the linker region in Figure 9 is hypothetical, it raises the question of whether the Gly-rich segment could effectively nucleate and stabilize the juxtamembrane coiled coil. The question is even more compelling when it is considered that the Gp7-FtsB$_{CC}$ construct has low thermal stability. Although the fusion protein crystallizes readily

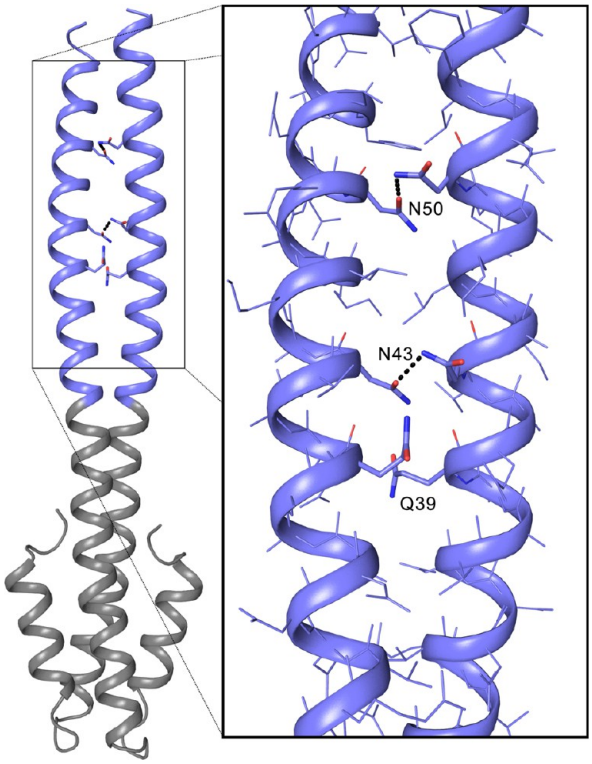

Figure 8. X-ray crystal structure of a Gp7-FtsB$_{CC}$ fusion protein. Ribbon representation of one of the two dimeric molecules in the asymmetric unit. This molecule forms a straight canonical coiled coil. The second molecule in the asymmetric unit exhibits a slight bend, possibly as a result of crystal packing (Supplementary Figure S2). The N-terminal Gp7 unit which replaces the transmembrane domain is highlighted in gray, and the FtsB sequence is in blue. The inset highlights a number of polar amino acids that are present at the interface in "*d*" (Q39) and "*a*" (N43 and N50) positions.

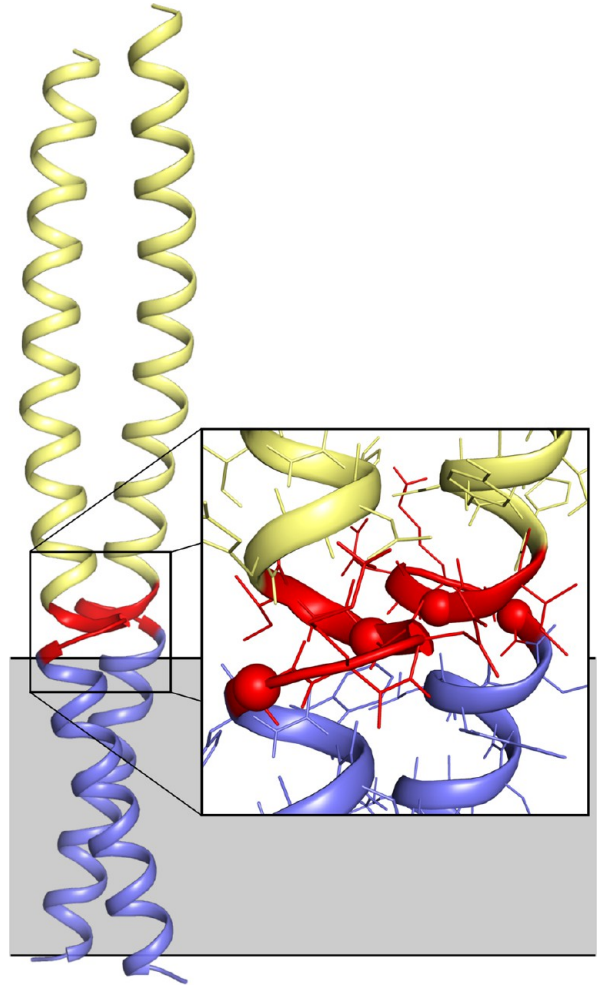

Figure 9. A theoretical model of a FtsB dimer that encompasses the transmembrane and coiled coil domains. The crystal structure of the coiled coil region of FtsB (yellow) and the computational Model 1 of the transmembrane domain (blue) were stitched together using a fragment based approach (see Materials and Methods). The resulting theoretical model includes a hinge between the coiled coil and the transmembrane helix where the helix unfolds (red). This hinge corresponds to conserved a Gly rich region in the sequence alignment (G21 and G25, spheres), suggesting that a flexible connection may be functionally important.

and is helical at low temperature, it reversibly unfolds quite rapidly, and it appears to be completely unfolded at 40 °C (Supplementary Figure S3). Longer constructs, including one that extends to the entire soluble region of FtsB, showed lower helicity and even lower stability. The relatively low stability of the coiled coil, however, is not surprising when it is considered that the structure includes a large number of polar amino acids (Q35, N43, N50) at the buried "*a*" and "*d*" positions, which are generally occupied by hydrophobic amino acids.[77,78] These sequence features appear conserved in the sequence alignment (Figure 7). Therefore, it is possible that association with FtsL may be required for the stabilization of the periplasmic region of FtsB. The fact that the periplasmic domain of FtsB may be partially unfolded could also account for some of the cellular instability of FtsB, which is rapidly degraded in the absence of FtsL.[16]

On the basis of our analysis, we hypothesize that a FtsB transmembrane homodimer forms an initial core that laterally recruits FtsL into a higher-order oligomer (Figure 10), likely a tetramer as proposed also by a recent bioinformatic analysis of the soluble domains.[36] Given the presence of several Thr residues in the TM helix of FtsL, an interesting possibility is that its lateral association could augment the membrane-embedded polar network by forming additional hydrogen bonds with the donor or acceptor groups that are left unsatisfied on Gln 16 (Figure 5a). The formation of the heterologous complex and the folding of the periplasmic domains may be a determinant for making FtsB competent for binding to the periplasmic domain of FtsQ,[16] which is required for their septal localization and the recruitment of the late proteins.

CONCLUSIONS

In this article, we have presented the first structural analysis of an integral membrane protein of the bacterial divisome. We demonstrate that the TM helix of FtsB self-associates in *E. coli* membranes. The interaction is mediated by an interhelical hydrogen bond formed by a critical polar residue embedded in the middle of the hydrophobic region. We also report the structure of the juxta-membrane domain of FtsB which forms a canonical coiled coil. The two domains are connected by a linker that is likely flexible. While the present study does not experimentally establish the precise oligomeric state of FtsB directly, the mutagenesis, modeling, and crystallographic data are consistent with the formation of a homodimer.

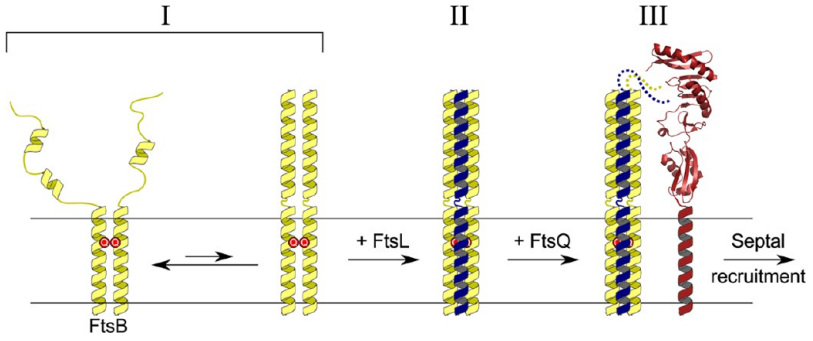

Figure 10. A functional hypothesis for the formation of the FtsB/FtsL complex and its recruitment to the divisome. The transmembrane domain of FtsB self-associates in *E. coli* membranes, driven by an interhelical hydrogen bond (Gln 16, represented by a red circle), but the coiled coil region is likely to be marginally stable or unstable (I). This finding raises the hypothesis that the interaction with FtsL is required to stabilize the periplasmic domain. It is likely that FtsL (blue) laterally associates with a pre-existing FtsB dimer (II). Alternatively, FtsL may compete with the self-association of FtsB to form an FtsB/FtsL heterodimer (not represented). Once the periplasmic domain is folded, the C-terminal tails of the FtsB/FtsL complex (dotted lines) would bind to FtsQ (red), and the proteins would subsequently be recruited to the division septum (III).

By defining the protein−protein interaction interface of FtsB and providing an experimentally validated structural model, the present work suggests the hypothesis that FtsB and FtsL assemble into a higher-order oligomer and sets the stage for the biophysical analysis of their heterologous complex. This study also establishes important groundwork for biological studies *in vivo* that will address whether the self-association of FtsB is essential for division and, specifically, whether the structural features identified here — the TM interaction interface, the Gly-rich linker and the stability of the coiled coil — are important for the localization of FtsB, for its association with FtsL, and for the recruitment of the other downstream proteins to the divisome.

■ ASSOCIATED CONTENT

Supporting Information

FtsB-TM computational models 1 and 2 (PDB files). X-ray crystallography statistics (Table S1). FtsB, complete sequence alignment (Figure S1). X-ray crystal structure of Gp7-FtsB$_{CC}$, two dimeric molecules in the asymmetric unit (Figure S2). CD analysis of Gp7-FtsB$_{CC}$ (Figure S3). This material is available free of charge via the Internet at http://pubs.acs.org.

Accession Codes

Coordinates and structure factors have been deposited in the Protein Data Bank with PDB ID code 4IFF.

■ AUTHOR INFORMATION

Corresponding Author

*Phone +1-608-890-2584; e-mail: senes@wisc.edu.

Funding

L.M.L. was supported by a WARF graduate fellowship. I.R. and K.C.T. were supported by funds from the NIH GM083987. Use of the Structural Biology ID19 beamline Argonne National Laboratory Advanced Photon Source was supported by the U.S. Department of Energy, Office of Energy Research, under Contract No. W-31-109-ENG-38.

Notes

The authors declare no competing financial interest.

■ ACKNOWLEDGMENTS

We are grateful to Dr. Darrell McCaslin of the Biophysical Instrumentation Facility of the Department of Biochemistry for assistance in the collection of the CD data. We thank Dr. Engelman and Miriam Alonso for providing the TOXCAT plasmids. We are grateful to Ben Mueller for useful discussion and assistance with TOXCAT, and to Dr. Vadim Klenchin for assistance with the QuikChange method. We thank Dr. Gevorg Gregorian for helpful discussion.

■ ABBREVIATIONS

TM: transmembrane

■ REFERENCES

(1) Adams, D. W., and Errington, J. (2009) Bacterial cell division: assembly, maintenance and disassembly of the Z ring. *Nat. Rev. Microbiol. 7*, 642−653.

(2) Mingorance, J., Rivas, G., Vélez, M., Gómez-Puertas, P., and Vicente, M. (2010) Strong FtsZ is with the force: mechanisms to constrict bacteria. *Trends Microbiol 18*, 348−356.

(3) Erickson, H. P., Anderson, D. E., and Osawa, M. (2010) FtsZ in bacterial cytokinesis: cytoskeleton and force generator all in one. *Microbiol. Mol. Biol. Rev. 74*, 504−528.

(4) Goehring, N. W., and Beckwith, J. (2005) Diverse Paths to Midcell: Assembly of the Bacterial Cell Division Machinery. *Curr. Biol. 15*, R514−R526.

(5) Szwedziak, P., Wang, Q., Freund, S. M., and Löwe, J. (2012) FtsA forms actin-like protofilaments. *EMBO J. 31*, 2249−2260.

(6) Shiomi, D., and Margolin, W. (2007) Dimerization or oligomerization of the actin-like FtsA protein enhances the integrity of the cytokinetic Z ring. *Mol. Microbiol. 66*, 1396−1415.

(7) Hale, C. A., Rhee, A. C., and De Boer, P. A. (2000) ZipA-induced bundling of FtsZ polymers mediated by an interaction between C-terminal domains. *J. Bacteriol. 182*, 5153−5166.

(8) Liu, Z., Mukherjee, A., and Lutkenhaus, J. (1999) Recruitment of ZipA to the division site by interaction with FtsZ. *Mol. Microbiol. 31*, 1853−1861.

(9) Sherratt, D. J., Arciszewska, L. K., Crozat, E., Graham, J. E., and Grainge, I. (2010) The Escherichia coli DNA translocase FtsK. *Biochem. Soc. Trans. 38*, 395−398.

(10) Mohammadi, T., Van Dam, V., Sijbrandi, R., Vernet, T., Zapun, A., Bouhss, A., Diepeveen-de Bruin, M., Nguyen-Distèche, M., De Kruijff, B., and Breukink, E. (2011) Identification of FtsW as a transporter of lipid-linked cell wall precursors across the membrane. *EMBO J. 30*, 1425−1432.

(11) Fraipont, C., Alexeeva, S., Wolf, B., Van der Ploeg, R., Schloesser, M., Den Blaauwen, T., and Nguyen-Distèche, M. (2011) The integral membrane FtsW protein and peptidoglycan synthase PBP3 form a subcomplex in Escherichia coli. *Microbiology (Reading, Engl.) 157*, 251−259.

(12) Nguyen-Distèche, M., Fraipont, C., Buddelmeijer, N., and Nanninga, N. (1998) The structure and function of Escherichia coli penicillin-binding protein 3. *Cell. Mol. Life Sci. 54*, 309−316.
(13) Bernhardt, T. G., and De Boer, P. A. J. (2003) The Escherichia coli amidase AmiC is a periplasmic septal ring component exported via the twin-arginine transport pathway. *Mol. Microbiol. 48*, 1171−1182.
(14) Heidrich, C., Templin, M. F., Ursinus, A., Merdanovic, M., Berger, J., Schwarz, H., De Pedro, M. A., and Höltje, J. V. (2001) Involvement of N-acetylmuramyl-L-alanine amidases in cell separation and antibiotic-induced autolysis of Escherichia coli. *Mol. Microbiol. 41*, 167−178.
(15) Gerding, M. A., Ogata, Y., Pecora, N. D., Niki, H., and De Boer, P. A. J. (2007) The trans-envelope Tol-Pal complex is part of the cell division machinery and required for proper outer-membrane invagination during cell constriction in E. coli. *Mol. Microbiol. 63*, 1008−1025.
(16) Gonzalez, M. D., and Beckwith, J. (2009) Divisome Under Construction: Distinct Domains of the Small Membrane Protein FtsB Are Necessary for Interaction with Multiple Cell Division Proteins. *J. Bacteriol. 191*, 2815−2825.
(17) Geissler, B., and Margolin, W. (2005) Evidence for functional overlap among multiple bacterial cell division proteins: compensating for the loss of FtsK. *Mol. Microbiol. 58*, 596−612.
(18) Buddelmeijer, N., Judson, N., Boyd, D., Mekalanos, J. J., and Beckwith, J. (2002) YgbQ, a cell division protein in *Escherichia coli* and *Vibrio cholerae*, localizes in codependent fashion with FtsL to the division site. *Proc. Natl. Acad. Sci. U. S. A. 99*, 6316−6321.
(19) Daniel, R. A., Harry, E. J., Katis, V. L., Wake, R. G., and Errington, J. (1998) Characterization of the essential cell division gene ftsL(yIID) of *Bacillus subtilis* and its role in the assembly of the division apparatus. *Mol. Microbiol. 29*, 593−604.
(20) Daniel, R. A., and Errington, J. (2000) Intrinsic instability of the essential cell division protein FtsL of *Bacillus subtilis* and a role for DivIB protein in FtsL turnover. *Mol. Microbiol. 36*, 278−289.
(21) Daniel, R. A., Noirot-Gros, M.-F., Noirot, P., and Errington, J. (2006) Multiple interactions between the transmembrane division proteins of *Bacillus subtilis* and the role of FtsL instability in divisome assembly. *J. Bacteriol. 188*, 7396−404.
(22) Bramkamp, M., Weston, L., Daniel, R. A., and Errington, J. (2006) Regulated intramembrane proteolysis of FtsL protein and the control of cell division in *Bacillus subtilis*. *Mol. Microbiol. 62*, 580−591.
(23) Wadenpohl, I., and Bramkamp, M. (2010) DivIC Stabilizes FtsL Against RasP Cleavage. *J. Bacteriol. 192*, 5260−5263.
(24) Ghigo, J. M., Weiss, D. S., Chen, J. C., Yarrow, J. C., and Beckwith, J. (1999) Localization of FtsL to the *Escherichia coli* septal ring. *Mol. Microbiol. 31*, 725−737.
(25) Katis, V. L., Wake, R. G., and Harry, E. J. (2000) Septal localization of the membrane-bound division proteins of Bacillus subtilis DivIB and DivIC is codependent only at high temperatures and requires FtsZ. *J. Bacteriol. 182*, 3607−3611.
(26) Buddelmeijer, N., and Beckwith, J. (2004) A complex of the Escherichia coli cell division proteins FtsL, FtsB and FtsQ forms independently of its localization to the septal region. *Mol. Microbiol. 52*, 1315−1327.
(27) Karimova, G., Dautin, N., and Ladant, D. (2005) Interaction network among Escherichia coli membrane proteins involved in cell division as revealed by bacterial two-hybrid analysis. *J. Bacteriol. 187*, 2233−2243.
(28) Robichon, C., Karimova, G., Beckwith, J., and Ladant, D. (2011) Role of leucine zipper motifs in association of the Escherichia coli cell division proteins FtsL and FtsB. *J. Bacteriol. 193*, 4988−4992.
(29) Goehring, N. W., Gueiros-Filho, F., and Beckwith, J. (2005) Premature targeting of a cell division protein to midcell allows dissection of divisome assembly in Escherichia coli. *Genes Dev. 19*, 127−137.
(30) Goehring, N. W., Gonzalez, M. D., and Beckwith, J. (2006) Premature targeting of cell division proteins to midcell reveals hierarchies of protein interactions involved in divisome assembly. *Mol. Microbiol. 61*, 33−45.
(31) Robichon, C., King, G. F., Goehring, N. W., and Beckwith, J. (2008) Artificial septal targeting of Bacillus subtilis cell division proteins in Escherichia coli: an interspecies approach to the study of protein-protein interactions in multiprotein complexes. *J. Bacteriol. 190*, 6048−6059.
(32) Rowland, S. L., Wadsworth, K. D., Robson, S. A., Robichon, C., Beckwith, J., and King, G. F. (2010) Evidence from Artificial Septal Targeting and Site-Directed Mutagenesis that Residues in the Extracytoplasmic {beta} Domain of DivIB Mediate Its Interaction with the Divisomal Transpeptidase PBP 2B. *J. Bacteriol. 192*, 6116−6125.
(33) Gonzalez, M. D., Akbay, E. A., Boyd, D., and Beckwith, J. (2010) Multiple interaction domains in FtsL, a protein component of the widely conserved bacterial FtsLBQ cell division complex. *J. Bacteriol. 192*, 2757−2768.
(34) Masson, S., Kern, T., Le Gouëllec, A., Giustini, C., Simorre, J.-P., Callow, P., Vernet, T., Gabel, F., and Zapun, A. (2009) Central domain of DivIB caps the C-terminal regions of the FtsL/DivIC coiled-coil rod. *J. Biol. Chem. 284*, 27687−27700.
(35) Noirclerc-Savoye, M., Le Gouëllec, A., Morlot, C., Dideberg, O., Vernet, T., and Zapun, A. (2005) In vitro reconstitution of a trimeric complex of DivIB, DivIC and FtsL, and their transient co-localization at the division site in Streptococcus pneumoniae. *Mol. Microbiol. 55*, 413−424.
(36) Villanelo, F., Ordenes, A., Brunet, J., Lagos, R., and Monasterio, O. (2011) A model for the Escherichia coli FtsB/FtsL/FtsQ cell division complex. *BMC Struct. Biol. 11*, 28.
(37) Russ, W. P., and Engelman, D. M. (1999) TOXCAT: A Measure of Transmembrane Helix Association in a Biological Membrane. *Proc. Natl. Acad. Sci. U. S. A. 96*, 863−868.
(38) Chen, G. J., Qiu, N., Karrer, C., Caspers, P., and Page, M. G. (2000) Restriction site-free insertion of PCR products directionally into vectors. *BioTechniques 28* (498−500), 504−505.
(39) Shaw, W. V. (1975) Chloramphenicol acetyltransferase from chloramphenicol-resistant bacteria. *Methods Enzymol. 43*, 737−755.
(40) Sulistijo, E. S., and Mackenzie, K. R. (2009) Structural basis for dimerization of the BNIP3 transmembrane domain. *Biochemistry 48*, 5106−5120.
(41) Blommel, P. G., and Fox, B. G. (2007) A combined approach to improving large-scale production of tobacco etch virus protease. *Protein Expr. Purif. 55*, 53−68.
(42) Otwinowski, Z., and Minor, W. (1997) [20] Processing of X-ray diffraction data collected in oscillation mode, in *Methods in Enzymology* (Charles, W. Carter, J., Eds.), pp 307−326. Academic Press.
(43) Morais, M. C., Kanamaru, S., Badasso, M. O., Koti, J. S., Owen, B. A. L., McMurray, C. T., Anderson, D. L., and Rossmann, M. G. (2003) Bacteriophage phi29 scaffolding protein gp7 before and after prohead assembly. *Nat. Struct. Biol. 10*, 572−576.
(44) Vagin, A., and Teplyakov, A. (2000) An approach to multi-copy search in molecular replacement. *Acta Crystallogr. D Biol. Crystallogr. 56*, 1622−1624.
(45) Cowtan, K. (2008) Fitting molecular fragments into electron density. *Acta Crystallogr. D Biol. Crystallogr. 64*, 83−89.
(46) Cowtan, K. (2010) Recent developments in classical density modification. *Acta Crystallogr. D Biol. Crystallogr. 66*, 470−478.
(47) Emsley, P., and Cowtan, K. (2004) Coot: model-building tools for molecular graphics. *Acta Crystallogr. D Biol. Crystallogr. 60*, 2126−2132.
(48) Murshudov, G. N., Vagin, A. A., Lebedev, A., Wilson, K. S., and Dodson, E. J. (1999) Efficient anisotropic refinement of macromolecular structures using FFT. *Acta Crystallogr. D Biol. Crystallogr. 55*, 247−255.
(49) Kulp, D. W., Subramaniam, S., Donald, J. E., Hannigan, B. T., Mueller, B. K., Grigoryan, G., and Senes, A. (2012) Structural informatics, modeling, and design with an open-source Molecular Software Library (MSL). *J. Comput. Chem. 33*, 1645−1661.
(50) Xiang, Z., and Honig, B. (2001) Extending the accuracy limits of prediction for side-chain conformations. *J. Mol. Biol. 311*, 421−430.

(51) Subramaniam, S., and Senes, A. (2012) An energy-based conformer library for side chain optimization: Improved prediction and adjustable sampling. *Proteins 80*, 2218−2234.
(52) Adams, P. D., Arkin, I. T., Engelman, D. M., and Brünger, A. T. (1995) Computational searching and mutagenesis suggest a structure for the pentameric transmembrane domain of phospholamban. *Nat. Struct. Biol. 2*, 154−162.
(53) Fleming, K. G., and Engelman, D. M. (2001) Computation and mutagenesis suggest a right-handed structure for the synaptobrevin transmembrane dimer. *Proteins 45*, 313−317.
(54) Jenei, Z. A., Warren, G. Z. L., Hasan, M., Zammit, V. A., and Dixon, A. M. (2011) Packing of transmembrane domain 2 of carnitine palmitoyltransferase-1A affects oligomerization and malonyl-CoA sensitivity of the mitochondrial outer membrane protein. *FASEB J. 25*, 4522−4530.
(55) Lemmon, M. A., Flanagan, J. M., Treutlein, H. R., Zhang, J., and Engelman, D. M. (1992) Sequence specificity in the dimerization of transmembrane alpha-helices. *Biochemistry 31*, 12719−25.
(56) Li, R., Gorelik, R., Nanda, V., Law, P. B., Lear, J. D., DeGrado, W. F., and Bennett, J. S. (2004) Dimerization of the transmembrane domain of Integrin alphaIIb subunit in cell membranes. *J. Biol. Chem. 279*, 26666−26673.
(57) Sulistijo, E. S., Jaszewski, T. M., and MacKenzie, K. R. (2003) Sequence-specific dimerization of the transmembrane domain of the "BH3-only" protein BNIP3 in membranes and detergent. *J. Biol. Chem. 278*, 51950−51956.
(58) Senes, A., Gerstein, M., and Engelman, D. M. (2000) Statistical analysis of amino acid patterns in transmembrane helices: the GxxxG motif occurs frequently and in association with beta-branched residues at neighboring positions. *J. Mol. Biol. 296*, 921−36.
(59) Senes, A., Chadi, D. C., Law, P. B., Walters, R. F. S., Nanda, V., and Degrado, W. F. (2007) E(z), a depth-dependent potential for assessing the energies of insertion of amino acid side-chains into membranes: derivation and applications to determining the orientation of transmembrane and interfacial helices. *J. Mol. Biol. 366*, 436−448.
(60) Senes, A., Engel, D. E., and DeGrado, W. F. (2004) Folding of helical membrane proteins: the role of polar, GxxxG-like and proline motifs. *Curr. Opin. Struct. Biol 14*, 465−479.
(61) Bowie, J. U. (2011) Membrane protein folding: how important are hydrogen bonds? *Curr. Opin. Struct. Biol 21*, 42−49.
(62) Joh, N. H., Min, A., Faham, S., Whitelegge, J. P., Yang, D., Woods, V. L., and Bowie, J. U. (2008) Modest stabilization by most hydrogen-bonded side-chain interactions in membrane proteins. *Nature 453*, 1266−1270.
(63) Choma, C., Gratkowski, H., Lear, J. D., and DeGrado, W. F. (2000) Asparagine-mediated self-association of a model transmembrane helix. *Nat. Struct. Biol. 7*, 161−6.
(64) Zhou, F. X., Cocco, M. J., Russ, W. P., Brunger, A. T., and Engelman, D. M. (2000) Interhelical hydrogen bonding drives strong interactions in membrane proteins. *Nat. Struct. Biol. 7*, 154−60.
(65) Fleming, K. G., and Engelman, D. M. (2001) Specificity in transmembrane helix-helix interactions can define a hierarchy of stability for sequence variants. *Proc. Natl. Acad. Sci. U. S. A. 98*, 14340−14344.
(66) Stanley, A. M., and Fleming, K. G. (2007) The role of a hydrogen bonding network in the transmembrane beta-barrel OMPLA. *J. Mol. Biol. 370*, 912−924.
(67) Li, E., You, M., and Hristova, K. (2006) FGFR3 dimer stabilization due to a single amino acid pathogenic mutation. *J. Mol. Biol. 356*, 600−612.
(68) Lawrie, C. M., Sulistijo, E. S., and MacKenzie, K. R. (2010) Intermonomer hydrogen bonds enhance GxxxG-driven dimerization of the BNIP3 transmembrane domain: roles for sequence context in helix-helix association in membranes. *J. Mol. Biol. 396*, 924−936.
(69) Partridge, A. W., Therien, A. G., and Deber, C. M. (2002) Polar mutations in membrane proteins as a biophysical basis for disease. *Biopolymers 66*, 350−358.
(70) Partridge, A. W., Therien, A. G., and Deber, C. M. (2004) Missense mutations in transmembrane domains of proteins: phenotypic propensity of polar residues for human disease. *Proteins 54*, 648−656.
(71) Lemmon, M. A., Treutlein, H. R., Adams, P. D., Brünger, A. T., and Engelman, D. M. (1994) A dimerization motif for transmembrane alpha-helices. *Nat. Struct. Biol. 1*, 157−163.
(72) Altschul, S. F., Gish, W., Miller, W., Myers, E. W., and Lipman, D. J. (1990) Basic local alignment search tool. *J. Mol. Biol. 215*, 403−410.
(73) Altschul, S. F., Madden, T. L., Schäffer, A. A., Zhang, J., Zhang, Z., Miller, W., and Lipman, D. J. (1997) Gapped BLAST and PSI-BLAST: a new generation of protein database search programs. *Nucleic Acids Res. 25*, 3389−3402.
(74) Frye, J., Klenchin, V. A., and Rayment, I. (2010) Structure of the tropomyosin overlap complex from chicken smooth muscle: insight into the diversity of N-terminal recognition. *Biochemistry 49*, 4908−4920.
(75) Klenchin, V. A., Frye, J. J., Jones, M. H., Winey, M., and Rayment, I. (2011) Structure-function analysis of the C-terminal domain of CNM67, a core component of the Saccharomyces cerevisiae spindle pole body. *J. Biol. Chem. 286*, 18240−18250.
(76) Costantini, S., Colonna, G., and Facchiano, A. M. (2006) Amino acid propensities for secondary structures are influenced by the protein structural class. *Biochem. Biophys. Res. Commun. 342*, 441−451.
(77) Harbury, P. B., Zhang, T., Kim, P. S., and Alber, T. (1993) A switch between two-, three-, and four-stranded coiled coils in GCN4 leucine zipper mutants. *Science 262*, 1401−1407.
(78) Grigoryan, G., and Keating, A. E. (2008) Structural specificity in coiled-coil interactions. *Curr. Opin. Struct. Biol. 18*, 477−483.